DOI: 10.1002/chem.201001875

A Neutral Zwitterionic Molecular Solid

Abdelkrim El-Ghayoury,[a] Cécile Mézière,[a] Sergey Simonov,[b] Leokadiya Zorina,[b] Manuel Cobián,[c] Enric Canadell,[c] Carme Rovira,[d, e] Bálint Náfrádi,[f] Balázs Sipos,[f] László Forró,[f] and Patrick Batail*[a]

Abstract: We report on the acid ethylenedithiotetrathiafulvaleneamidoglycine (EDT-TTF-CO-NH-CH_2-CO_2H; **1**; EDT-TTF = ethylenedithiotetrathiafulvalene) and the 1:1 adduct [(EDT-TTF)$^{\cdot+}$-CO-NH-CH_2-$(CO_2)^-$][(EDT-TTF)-CO-NH-CH_2-(CO_2H)]·CH_3OH (**2**), a new type of hydrogen-bonded, 1:1 acid/zwitterion hybrid embrace of redox peptidics into a two-dimensional architecture, an example of a system deliberately fashioned so that oxidation of π-conjugated cores toward the radical-cation form would interfere with the activity of the appended ionizable residues in the presence of a templating base during crystal growth. First-principles calculations demonstrate that, notwithstanding preconceived ideas, a metallic state is more stable than the hole-localized alternatives for a neat 1:1 neutral acid/zwitterion hybrid. The inhomogeneous Coulomb field associated with proton-shared, interstacks O−H···O hydrogen bonds between the ionizable residues distributed on both sides of the two-dimensional π-conjugated framework leads, however, to a weak hole localization responsible for the activated but high conductivity of 1 $S\,cm^{-1}$. This situation is reminiscent of the role of the environment on electron transfer in tetraheme cytochrome *c*, in which the protonation state of a heme propionate becomes paramount, or ion-gated transport phenomena in biology. These observations open rather intriguing opportunities for the construction of electronic systems at the interface of chemistry and biology.

Keywords: electron transport · electronic structure · peptides · template synthesis · zwitterions

Introduction

The research reported herein was seen at its onset as a materials-discovery initiative designed to explore the outcome of competing hydrogen-bonding interactions in directing the stoichiometry and structure of solids based on ethylenedithiotetrathiafulvaleneamidoglycine (EDT-TTF-CO-NH-CH_2-CO_2H; **1**; EDT-TTF = ethylenedithiotetrathiafulvalene) a TTF core bearing an ionizable amino acid residue (i.e., glycine (Gly)),[1,2] when associated with conjugated carboxylates,[3] chosen herein to serve as templating bases. Our goal was to fashion a system whereby redox activation of π-conjugated cores toward their radical-cation forms would interfere with the association/dissociation of protons at the acid/base interface during crystal growth[4] in nonaqueous solvents, in much the same way that the anionic charge is tuned by even a fraction of one unit as a direct effect of the microenvironment on the pK_a value of the ionizable side group in large membrane proteins[5] or that charge transfer, redox processes, and hole migration in a network are affected by collective hydrogen-bond activation[6–8] and dynamics.[9,10] By choosing to append a π-conjugated system with

[a] Dr. A. El-Ghayoury, C. Mézière, Dr. P. Batail
Laboratoire MOLTECH-Anjou
CNRS, Université d'Angers
49045 Angers (France)
E-mail: patrick.batail@univ-angers.fr

[b] Dr. S. Simonov, Dr. L. Zorina
Institute of Solid State Physics RAS
142432 Chernogolovka MD (Russia)

[c] Dr. M. Cobián, Dr. E. Canadell
Institut de Ciència de Materials de Barcelona (ICMAB-CSIC)
Campus de la UAB, 08193, Bellaterra (Spain)

[d] Dr. C. Rovira
Parc Cientific de Barcelona and IQTCUB
Josep Samitier 1-5, 08028 Barcelona (Spain)

[e] Dr. C. Rovira
Institució Catalana de Recerca i Estudis Avançats
Passeig Lluís Companys 23, 08018 Barcelona (Spain)

[f] Dr. B. Náfrádi, Dr. B. Sipos, Prof. L. Forró
Institut de Physique de la Matière Complexe
Ecole Polytechnique Fédérale de Lausanne (EPFL)
1015 Lausanne (Switzerland)

Supporting information for this article is available on the WWW under http://dx.doi.org/10.1002/chem.201001875.

an amino acid, a complementary objective was to take advantage of the structure-directing ability of peptide residues prone to self-organization in a manner that mimics natural processes[11] by stabilizing robust patterns of intermolecular interactions, such as β-strand and sheet motifs,[12–15] thereby creating situations in which the former will compete, and ultimately compromise, with π–π interactions between neutral redox cores and between their radical-cation forms.

Herein, we report a new type of hydrogen-bonded 1:1 acid/zwitterion hybrid embrace of redox peptidics into a two-dimensional architecture as an example of a system deliberately fashioned so that oxidation of π-conjugated cores toward their radical-cation form would interfere with the activity of their appended ionizable residues in the presence of a templating base during crystal growth. First-principles calculations demonstrate that, notwithstanding preconceived ideas, a metallic state is more stable than the hole-localized alternatives for a neat 1:1 neutral acid/zwitterion hybrid. The inhomogeneous Coulomb field associated with proton-shared, interstacks O–H···O hydrogen bonds between the ionizable residues distributed on both sides of the two-dimensional π-conjugated framework leads, however, to a weak hole localization responsible for the activated but high conductivity. This situation is reminiscent of the role of the environment on electron transfer in tetraheme cytochrome *c*, in which the protonation state of a heme propionate becomes paramount, or ion-gated transport phenomena in biology. These observations open rather intriguing opportunities for the construction of electronic systems at the interface of chemistry and biology.

Results and Discussion

Templated electrocrystallization of a layered 1:1 neutral/zwitterionic solid: The successful growth of crystals of acid **1** suitable for X-ray diffraction studies (Table 1) provided the desirable opportunity to identify the pattern of intermolecular interactions in the solid state for the redox acid in its neutral state. The structure of **1** reveals a pattern of association typical of a β-strand infinite motif and the stabilization of hydrogen-bonded carboxylic acid dimers (Figures 1 and 2). As radical-cation salts are grown electrochemically in nonaqueous solvents, we decided to set up electrocrystallization cells with $Bu_4N^+[HO_2C{-}CH{=}CH{-}CO_2]^-$ as both a templating base and the electrolyte. Thus, the balance of the chemical activity during crystal growth would ultimately rule an outcome that favored either a two-component radical-cation salt (i.e., $[EDT\text{-}TTF\text{-}CO\text{-}NH\text{-}CH_2\text{-}CO_2H]_n^{\bullet+}$ ($HO_2C\text{-}CH{=}CH\text{-}CO_2^-$)) or the monomolecular zwitterionic form (i.e., $[(EDT\text{-}TTF)^{\bullet+}\text{-}CO\text{-}NH\text{-}CH_2\text{-}(CO_2)^-]$) instead.

The zwitterionic form is identified in the structure (Table 1) of the black platelike crystals harvested on the anode with no evidence for the presence of the fumarate anion. Hence, the latter turned out to be a base strong enough to ionize the Gly residue. Remarkably, the zwitterion is engaged in a bimolecular embrace with one molecule of the neutral acid, an association, thereafter called the peptidic dimer, driven by hydrogen bonding between the two self-complementary Gly residues (Figure 3). Hence, the bent, flexible neutral core is directed to embrace the flattened and rigidified radical-cation core in a face-to-face configuration, thus yielding the 1:1 adduct $[(EDT\text{-}TTF)^{\bullet+}\text{-}CO\text{-}NH\text{-}CH_2\text{-}(CO_2)^-][(EDT\text{-}TTF)\text{-}CO\text{-}NH\text{-}CH_2\text{-}(CO_2H)]\cdot CH_3OH$ (**2**). This result shows that the chemical potential of the templating base needs to be properly tuned to make the zwitterionic form and its conjugated acid both available during crystal growth. In hindsight, this remarkable outcome appears to be entirely consistent with unsuccessful attempts at electrocrystallization of the zwitterion directly from $(Bu_4N^+)[EDT\text{-}TTF\text{-}CO\text{-}NH\text{-}CH_2\text{-}(CO_2)^-]$. Note that the few known examples of tetrathiafulvalene zwitterions are either based on phosphonates[16] or imidazoles;[17,18] in addition, quaterthiophene–peptide hybrid systems recently synthesized did not exhibit any π–π interactions between the oligothiophene segments.[19]

Table 1. Crystallographic and refinement data for **1** and **2** at room temperature.

	1	**2**
chemical formula	$C_{11}H_9NO_3S_6$	$C_{23}H_{21}N_2O_7S_{12}$
M_r	395.55	822.14
crystal system	monoclinic	monoclinic
a [Å]	8.511(1)	12.8611(7)
b [Å]	18.397(2)	14.661(1)
c [Å]	10.0007(6)	16.963(1)
β [°]	99.635(7)	101.233(5)
V [Å^3]	1543.8(3)	3137.1(4)
space group, Z	$P\,2_1/c$,4	$P\,2_1/a$,4
ρ_{calcd} [g cm^{-3}]	1.702	1.741
μ [cm^{-1}]	8.92	8.83
F(000)	808	1684
θ range [°]	3.62–26.49	3.67–29.00
indices ranges	$-10\le h\le 10$	$-13\le h\le 17$
	$-23\le k\le 21$	$-19\le k\le 20$
	$-12\le l\le 12$	$-23\le l\le 23$
reflections collected	15810	51736
independent reflections	3163	8183
R_{int}	0.0519	0.0654
no. of variables	217	463
GOOF on F^2	1.032	1.010
final $R[I>2\sigma(I)]$	0.0473	0.0494

Three geometrical features qualify the difference between the neutral acid molecule and the zwitterionic form in the peptidic dimer, namely, the localization of the acid proton, the charge-dependent bending of the EDT–TTF cores, and the length of their inner C=C bonds, which should be expected to increase upon oxidation because the p_π orbitals of the inner carbon atoms are in a bonding combination within the HOMO of the TTF core. Thus, the lack of a proton and an elongated inner C=C bond at 1.371(3) Å (compare with 1.334(4) Å for the neutral acid **1**) qualify the lower molecule in Figure 3a as primarily the zwitterionic form. Conversely, the identification and refinement of the carboxylic acid proton and a shorter inner C=C double bond at 1.356(4) Å qualify the second molecule as primarily the neutral, pure acid form. Yet, it is of interest to note that these C=C bonds

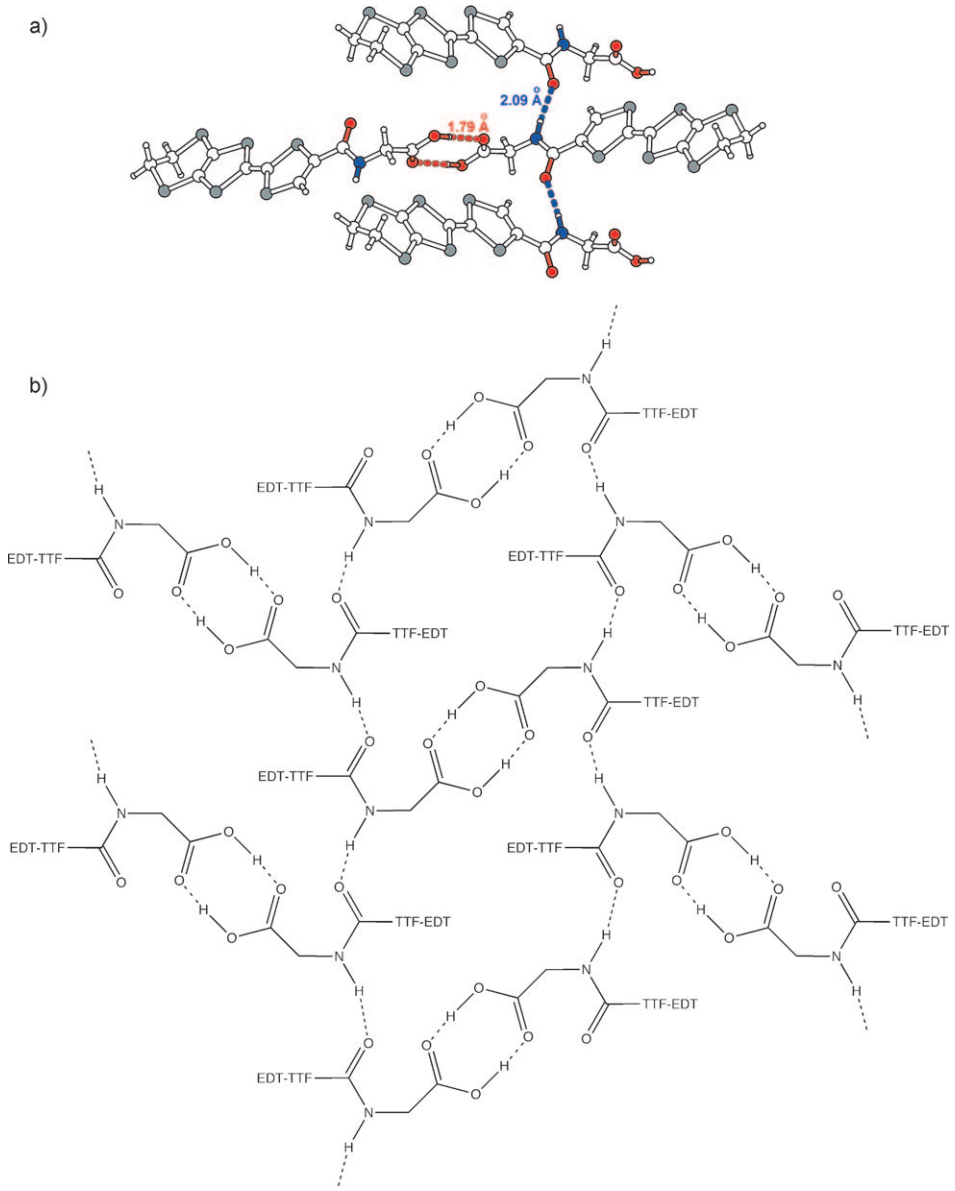

Figure 1. Structure of EDT-TTF-CO-NH-CH_2-CO_2H (**1**). a) The primary packing motif of **1** is based on one O–H···O bond (Table 2), thus forming a typical carboxylic dimer unit and one N–H···O bond (Table 2) and generating an infinite β-strand motif, both also illustrated in a projection along the *a* axis in Figure 2. b) Schematic representation of the pattern of intermolecular association.

are not quite as long or short as they should respectively be for purely charged or neutral TTF cores. Note in addition that the dihedral angles between the TTF core C2S4 fragment and the outer six- and five-membered rings in the acid are twice as large of those angles in the zwitterion, that is, 9.01(3) and 11.65(5)° for the six- and five-membered rings relative to 4.14(5) and 6.13(4)°, respectively. These angles amount to 5.43(5) and 4.61(8)° for **1**. Hence, the charge-poor molecules are bent and charge-rich molecules are flattened, as expected.[20] The dual embrace of the Gly residues is stabilized by two intradimer hydrogen bonds, with distances that are typical of such peptide bonds,[11] that is, *d*(H···O) = 2.02(4) and 2.02(4) Å and *d*(N···O) = 2.849(3) and 2.795(3) Å and angles of N–H···O = 174(4) and 161(4)° (Table 2). Peptidic dimers stack along the *b* axis such that alternating TTF cores are essentially eclipsed and equidistant at 3.6–3.7 Å and the stacks associate into *a*–*b* slabs (see Figure 5), which have an interface along the *c* axis that defines pockets (Figure 4) where pairs of hydrogen-bonded methanol molecules are captured and stabilized over two disordered positions with half-occupancy.

The interstacked interdimer O–H···O hydrogen bond, with an O···O distance as short as 2.459(3) Å, may be considered to be a proton-shared chemical bond,[21] that is, this hydrogen atom may be seen as bonded to both oxygen atoms (exemplified and drawn in red in Figure 5). A low-energy barrier between a double-minimum potential is calculated for a O···O separation of 2.46 Å,[22] thus indicating that O–H···O and O···H–O configurations are possible, yet the structural refinement is more in favor of one of the two configurations in which the proton is primarily connected to the neutral acid (the corresponding O–H bond length is 1.03 Å and the H···O distance is 1.43 Å; Table 2).

Note that the C–O bond lengths for the two oxygen atoms involved in the proton-shared hydrogen bond remain close to 1.308(4) Å, the value found for the single C–O bond in **1** regardless of whether the oxygen atom of the neutral acid or the zwitterion (1.277(3) and 1.289(3) Å, respectively) are engaged between any two peptidic dimers, and that they are longer than the two adjacent double C=O bonds (1.220(3) Å in both molecules relative to 1.201(4) Å in **1**).

Table 2. Hydrogen bonds in **1** and **2**.

Compound/ molecule	D–H···A[a]	D–H [Å]	H···A [Å]	D···A [Å]	D–H···A [°]
1	$O–H_{acid}···O_{acid}$	0.95(5)	1.79(5)	2.712(4)	163(4)
	$N–H_{amide}···O_{amide}$	0.83(2)	2.09(2)	2.911(3)	168(3)
2/neutral	$O–H_{acid}···O_{acid}$	1.03(5)	1.43(5)	2.459(3)	175(4)
	$N–H_{amide}···O_{acid}$	0.84(3)	2.02(4)	2.849(3)	174(4)
2/zwitterion	$N–H_{amide}···O_{acid}$	0.81(4)	2.02(4)	2.795(3)	161(4)

[a] D = donor, H = hydrogen atom, A = acid.

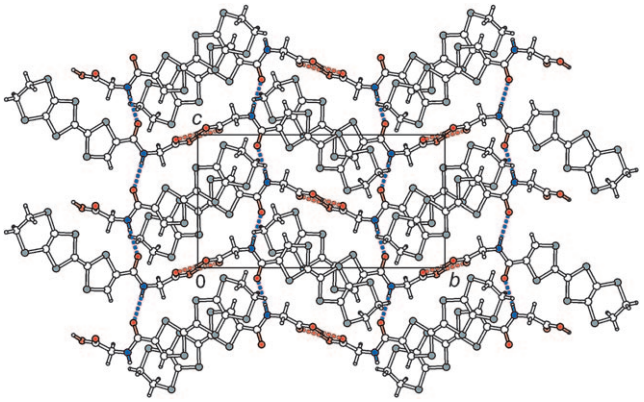

Figure 2. The combination of the two hydrogen-bonding motifs in **1**, described in Figure 1, efficiently templates infinite stacks in which neutral molecules are related by inversion along the *a* axis. Note that molecules from adjacent stacks along the *b* axis are not parallel, the dihedral angle between the mean planes of their TTF cores amounts to 64.04(2)°.

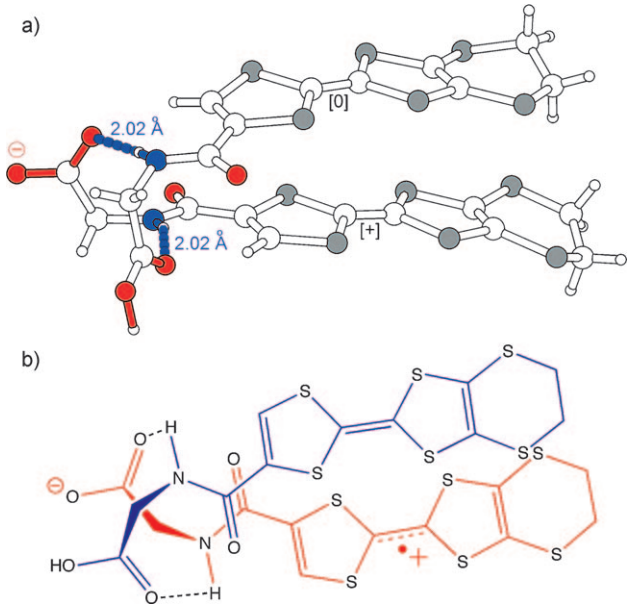

Figure 3. Peptidic dimer in $[(EDT\text{-}TTF)^{\bullet+}\text{-}CO\text{-}NH\text{-}CH_2\text{-}(CO_2)^-][(EDT\text{-}TTF)\text{-}CO\text{-}NH\text{-}CH_2\text{-}(CO_2H)]\cdot CH_3OH$ (**2**). a) The self-complementary hydrogen-bond association of the two Gly residues brings together the molecules into a 1:1 adduct. Note that the lower molecule is in a flattened, primarily zwitterionic form, whereas the upper molecule is in a bent, primarily neutral state. The peptide units are in a folded arrangement instead of parallel,[14] thereby allowing for the π-conjugated cores to face each other within the dimer. b) Within the dimer, the neutral acid is shown in blue and the zwitterionic form in red. Interestingly, both O atoms of the C=O groups covalently linked to the TTF core (C=O: 1.221(3) Å) in **2** are less active than in **1** because they are only engaged in weak C–H···O contacts with guest methanol molecules. The negative-charge distribution within the acid/base, carboxylic/carboxylate fragments is inherent to the fate of the outer proton that belongs to the ionizable residue on the outskirts of the peptidic dimer, as discussed in the text and Figure 5.

These bond lengths are useful in probing the charge distribution in the *a*–*b* layers because they demonstrate that the negative charges located in the vicinity of interstacks, proton-shared hydrogen-bonding $[O\text{–}H\cdots O]^-$ units are close

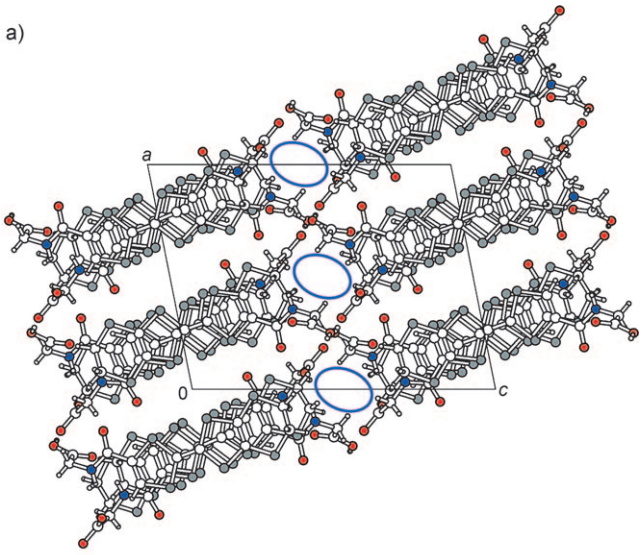

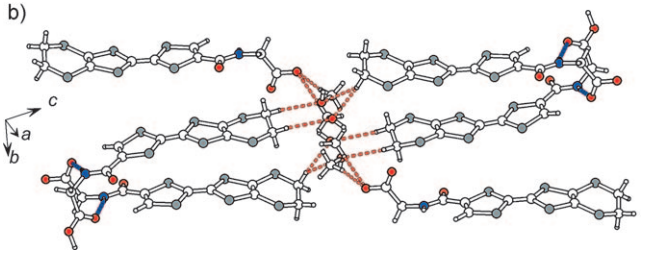

Figure 4. A projection of a fragment of two *a*–*b* slabs with methanol pockets at their interface in **2**. Note the striking difference between the structure of the orange–red crystals of the pure amino acid form **1** (shown in Figure 2) and that of the black crystals of **2** (shown here in the upper illustration).

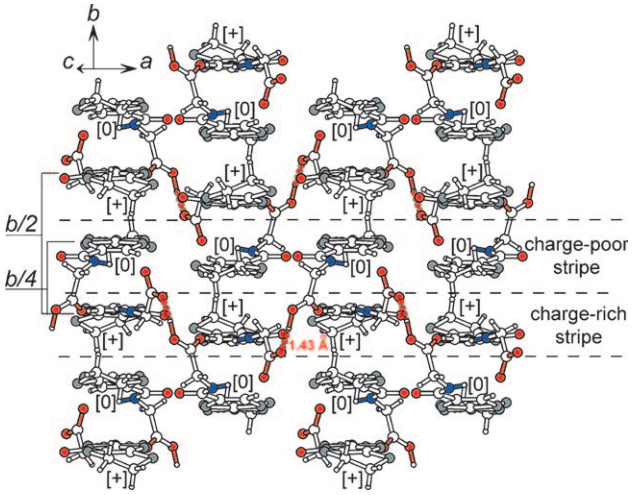

Figure 5. Hydrogen-bonding framework that envelopes both sides of the two-dimensional π-conjugated network in $[(EDT\text{-}TTF)^{\bullet+}\text{-}CO\text{-}NH\text{-}CH_2\text{-}(CO_2)^-][(EDT\text{-}TTF)\text{-}CO\text{-}NH\text{-}CH_2\text{-}(CO_2H)]\cdot CH_3OH$. Stacks of overlapping peptidic dimers develop along the *b* axis and are coupled along the *a* axis by a strong interdimer O–H···O hydrogen bond (drawn in red), which defines the acid/base interface in the crystal. The primarily charged and primarily neutral TTF cores are labeled with [+] and [0], respectively. Within a layer, charge-rich and charge-poor stripes alternate along the *b* axis between thin dashed lines. The *b*/2 and *b*/4 periodicities are discussed in the text.

to positively charged {EDT−TTF}$^+$ units, thereby defining charge-rich and charge-poor stripes alternating along the *b* axis (Figure 5).

An important outcome of the former analysis of the molecular-geometry data lies in the identification of a *b*/4 periodicity for the alternation of the TTF cores, whereas the negatively charged [O−H···O]$^-$ units are translated with a *b*/2 periodicity instead. Hence, to the extent that sharing a proton within collections of [O···H···O]$^-$ bonds provides a mechanism for balancing the chemical potential at the acid–base interface in the solid state, effectively smoothing out the electrostatic interactions in the environment of the π-conjugated cores, this acts as an additional potential akin to that ascribed to anion ordering in 2:1 mixed valence radical-cation salts.

Highly conducting yet localized: The electron spin resonance (ESR) signal shows that the spins are bound into a singlet configuration, and a thermal energy of 350 K is required to excite spins into the triplet state as detected by ESR spectroscopic analysis (Figure 6). From the fit of single–triplet activation (Figure 6) there is roughly one spin dimer per two peptidic dimers. The spin-singlet formation

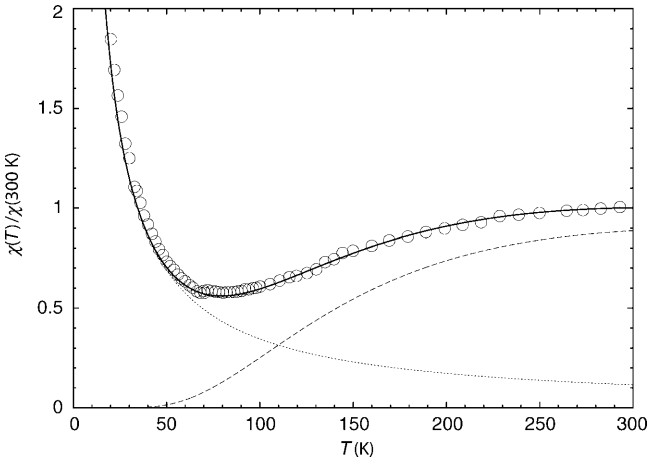

Figure 6. Temperature dependence of the spin susceptibility relative to its room-temperature value measured by ESR spectroscopy at 9.4 GHz. The solid (circled) line is a superposition of a thermally excited paramagnetic spin with a spin gap of $\Delta = 350$ K (dashed line) and an impurity Curie component (dotted line) of about 2% concentration.

hinders the coherent charge transport. The temperature dependence of the resistivity shows activated behavior from room temperature to approximately $T \approx 125$ K with a single-particle gap of $\Delta = 620$ K (Figure 7). Despite the charge localization, one has a sizeable room-temperature conductivity of 1 S cm^{-1}.

Electronic-structure calculations favor a metallic character: The association of collections of peptidic dimers into a two-dimensional topology calls for electronic-structure calculations to analyze whether the dimers interact with each other along the *a* and *b* axes. We have thus calculated the different

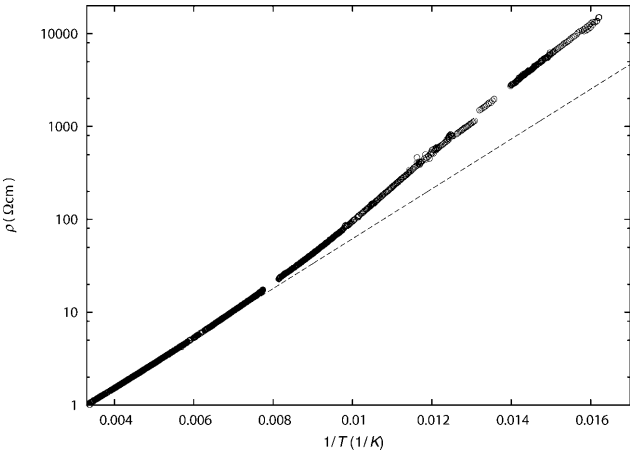

Figure 7. Arrhenius plot of the resistivity for **2**. A thermally activated temperature dependence of the resistivity (circled line) is identified in the temperature range $T = 125$–300 K. The dashed line shows a calculated thermally activated behavior with a single-particle gap $\Delta = 620$ K and room-temperature conductivity of $\sigma_0 = 1$ S cm^{-1}. A small deviation from a simple activated like temperature dependence is present below 125 K.

$\beta_{HOMO/HOMO}$ interaction energies,[23] which are a sensitive measure of the strength of the different HOMO/HOMO interactions in the lattice (see Figure 8 for labeling). The interaction energies for the intra- and interdimer interactions along the *b* axis are strong, whereas the energies along the

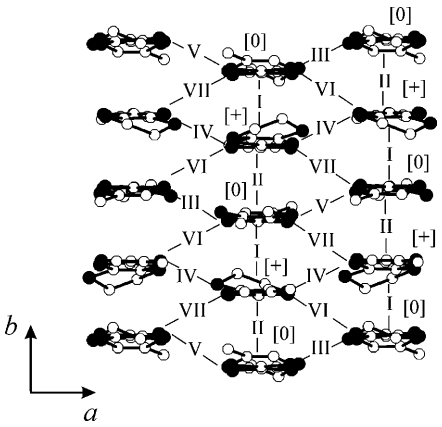

Figure 8. One layer in **2** viewed down the *c** axis. Note that the Gly residues have been removed for clarity. The different types of intermolecular interactions are labeled I–VII. Interaction II = intradimer interaction.

direction of the interstacks are one order of magnitude weaker (Table 3). As a result, the calculated extended Hückel tight-binding band structure (Figure 9) is typical of a metallic system with a larger dispersion along the direction of the stacks. However, because the two components of the peptidic dimer are chemically very different, the tight-binding calculations could not be accurate enough. In addition, explicit consideration of electronic repulsions is important to test the possibility of localized nonmetallic states. Thus, we have carried out first-principles DFT calculations for the metallic state and for different alternative states in which

Table 3. Absolute values of the $\beta_{HOMO-HOMO}$ interaction energies and S···S distances shorter than 4.0 Å for the different intermolecular interactions in one layer of **2** at room temperature.

Interaction[a]	S···S [Å]	$\lvert\beta_{HOMO-HOMO}\rvert$ [eV]
I	3.6302, 3.6317, 3.7052, 3.7750, 3.9014	0.5485
II (intra-dimer)	3.778, 3.782, 3.837, 3.946, 3.995	0.3758
III	3.667 (×2), 3.742 (×2)	0.0113
IV	3.3025, 3.4032, 3.9031, 3.9459	0.0292
V	3.598 (×2)	0.0020
VI	3.9115	0.0629
VII	(4.0924, 4.0994)	0.0593

[a] See Figure 8 for the labeling.

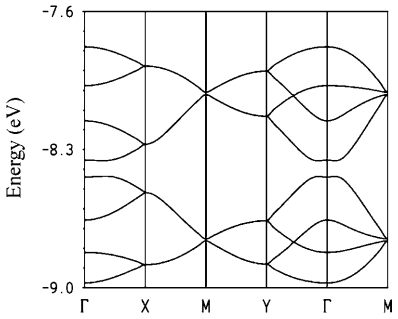

Figure 9. Extended Hückel band structure in the region of the HOMO bands for layers of **2**. $\Gamma=(0, 0)$, $X=(a^*/2, 0)$, $Y=(0, b^*/2)$, $M=(a^*/2, b^*/2)$, and $S=(-a^*/2, b^*/2)$. There are four holes in the system; therefore, the system should be metallic.

holes are localized onto the zwitterionic partners instead. The metallic state is more stable than the hole-localized alternatives. The calculated band structure for this metallic state is shown in Figure 10, in which the eight bands result from a strong mixing of the HOMOs of both the neutral and zwitterionic partners. The upper four bands are slightly more heavily based on the zwitterionic units, whereas the reverse is true for the lower four bands, in agreement with the

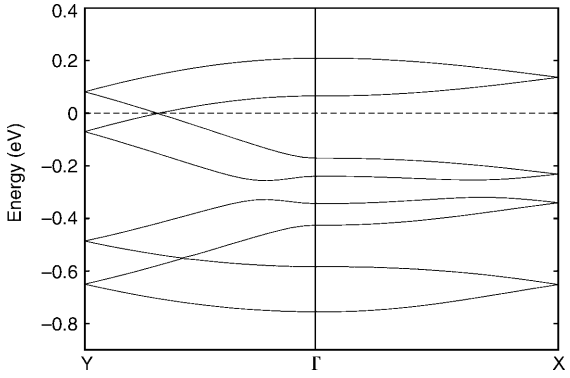

Figure 10. DFT band structure for the metallic state of **2** represented along the a^* and b^* axes. The dashed line indicates the Fermi level and Γ, X, and Y refer to the (0, 0, 0), ($a^*/2$, 0, 0), and (0, $b^*/2$, 0) points of the monoclinic reciprocal lattice.

chemical description. Hence, the first-principles calculations completely confirm the extended Hückel band structure (bandwidth, nature of the bands, avoided crossings, and so forth) and clearly show the strong tendency for the holes to delocalize from the zwitterionic HOMOs.

Electrostatic potentials: To further consider the tendency of the holes to delocalize, an important outcome in the context of this study, we also calculated the electrostatic potential of the peptidic dimer and the isolated constituents (i.e., the acid and zwitterion). We recall that the intradimer interaction is the weaker of the two interactions along the stacks (Table 3 and Figure 8). The study was carried out by means of B3LYP-DFT//6-31G* calculations, that is, by using an atomic-orbital basis set in contrast with the plane-wave-type calculations employed for the band-structure calculations. The calculated electrostatic potentials for the isolated acid and zwitterionic partners are shown in Figure 11a,b, respectively. The existence of the delocalized positive charge on the π system of the zwitterion is clearly seen (for example, compare the light-blue contours around the middle of the central C=C bond or on top of the six-membered ring). We have given the values of the electrostatic potential for the S and C atoms of the central TTF core in Table 4 to put this finding on a more quantitative basis. The calculated values for these atoms in the isolated zwitterion are around +0.10 atomic units higher than in the isolated acid.

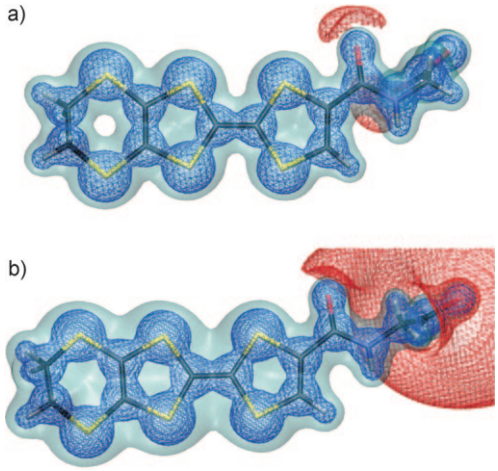

Figure 11. Surfaces of constant electrostatic potential calculated for the isolated acid (a) and zwitterionic (b) partners of the peptidic dimer. The electrostatic potentials are −0.07 (red), +0.2 (light blue), and +0.6 (dark blue) atomic units.

In addition, the values for the electrostatic potentials when the acid and zwitterion face each other in the dimer are also shown in Table 4. It is striking that the values for a given atom in the two partners are very similar, with values intermediate between those of the two isolated species. This outcome clearly shows that the positive charge is almost equally shared between the π systems of the two partners of the dimer. Note that the calculated unpaired spin density is

Table 4. Calculated values of the electrostatic potential (atomic units) for the S and C atoms of the central TTF core of the acid and zwitterionic partners of the peptidic dimer both isolated and within the dimer.

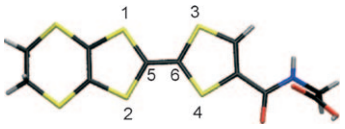

Positions	Isolated acid	Acid in the dimer	Zwitterion in the dimer	Isolated zwitterion
1	−59.14671	−59.09456	−59.10128	−59.04074
2	−59.15621	−59.09442	−59.10506	−59.04120
3	−59.16231	−59.12352	−59.12599	−59.07374
4	−59.17868	−59.11088	−59.12908	−59.06241
5	−14.67911	−14.62116	−14.63225	−14.56629
6	−14.69831	−14.63249	−14.64296	−14.57609

also shared almost equally by the two partners (49 and 51 % in the zwitterion and acid, respectively). Thus, these results confirm by means of a different approach the strong tendency of the holes to delocalize along the TTF cores of the two different species of this solid.

A shared positive charge: The analysis of the electrostatic potentials of the dimer and its two constituents demonstrates that the positive charge is strongly shared by the π systems of the two partners within the dimer. The reason for this surprising result is the very good face-to-face intermolecular overlap along the stacks brought about by the intra- and interdimer hydrogen bonds, thus allowing for strong interaction of the HOMOs of the two partners, which overrides the energy difference between the two different types of HOMOs. Such a hole delocalization explains in a natural way the elongated inner C=C central bond of the neutral molecule with respect to this bond in the neutral acid **1** and the relatively short C=C central bond of the zwitterion with respect to these bonds in typical TTF-like radical cations (see legend for Figure 3). We are thus led to the intriguing conclusion that a metallic state should be favored for the ordered layer of the alternating, segregated zwitterionic and neutral molecules illustrated in Figure 5.

The first-principles electronic structure studies are based on two different approaches: plane-wave-based DFT calculations with a generalized gradient approximation (GGA)-type exchange–correlation functional for the band structure and ab initio atomic-orbital-based DFT calculations with a B3LYP-hybrid-type functional for the electrostatic potentials. Thus, the essential result of these studies, namely, a large zwitterion/neutral molecule hole delocalization, must be essentially correct. Yet, the electrons are in fact localized and the system clearly shows activated conductivity. How to integrate these seemingly contradictory observations into a consistent scenario? Note that without a large hole delocalization it would not be easy to understand the high conductivity of the system, even if it is activated. A truly localized picture in which a series of zwitterions with localized holes are segregated within a series of neutral molecules can only lead to a strong insulator. Therefore, the delocalization predicted by the theoretical approaches may be somewhat overestimated but not openly wrong.

Because the only parameter in the calculations is the crystal structure, one is entitled to suspect that one feature of the crystal structure may primarily lead to over-delocalization. The degree of delocalization is essentially proportional to the overlap integral between the HOMOs of the two species and is inversely proportional to their energy difference. The overlap integrals, which mostly depend on the overlap mode, are very strong along the stacks and are considerably weaker along the interstack region (exactly as the $\beta_{HOMO/HOMO}$ interaction energies of Table 3). Because the network is highly constrained by hydrogen bonds (Figure 5), the main control parameter to probe and adjust in the crystal structure is the central C=C length. Note however that the overlap remains large regardless of the value of the bond length. Thus, the energy difference between the HOMOs of the zwitterion and neutral molecule, instead of the strength of the overlap, remains the key factor in explaining the possible overestimation of the delocalization. As noted above, the proton-shared, interdimer O−H···O hydrogen bond is such that it is not simple to know if the hydrogen atom, and thereby the negative charge, is associated with one or the other units. This finding means that if the anion-charge localization and the π-type electrons are not largely independent, the central C=C length on each molecular site, which is longer for charged units, may be an average. If this is so, the present C=C lengths are more similar than they should be; consequently, the HOMO energies are too close and the interaction between the HOMOs is too strong, thus leading to an exaggerated delocalization. However, as discussed above, the charge-sensitive shape of the π-conjugated inner cores does not indicate that the averaging due to the proton-shared hydrogen-bond manifold is really significant. Thus, we conclude that the tendency of the holes to delocalize is a real feature and that the key to understanding the weak localization must lie outside the geometrical details of the inner TTF cores of the molecules.

A nonuniform Coulomb potential associated with a proton-shared hydrogen bond: We believe that a more likely explanation of the activated conductivity is not the overestimation of the delocalization but the following: If a metallic state exists for the system, its inherent hole delocalization would force central C=C lengths to be longer than usual for the neutral partner and shorter than usual for the zwitterionic partner, exactly as found in the actual crystal structure. Thus, the DFT calculations bring to the fore that a metallic state is perfectly compatible with the crystal structure if no additional potential, not included in the calculations, tends to localize the carriers. Indeed, because of the nature of the interstacks, proton-shared hydrogen bonds, a nonuniform extra Coulomb potential envelops both sides of the two-dimensional π-conjugated framework (Figure 5), and yet this potential is not taken into account in any periodic calculation based on the eight-donor repeat cell (i.e., the necessarily averaged crystal structure). We believe that the metallic

state revealed for the model-ordered layer of segregated zwitterionic and neutral molecules is not stable under this additional inhomogeneous potential in the environment[24–26] of the real layers, thus leading to the weak hole localization responsible for the activated but high conductivity. Note that the disorder associated with the rattling proton also affects the interstacks interactions, thus most likely influencing the spin gap and the susceptibility behavior. It follows that the hydrogen atoms of the interstacks, proton-shared O–H···O hydrogen bonds, which are not part of the conducting network of the system, are imposing the collective behavior of the mobile electrons, a situation reminiscent of the role of the environment on electron transfer in tetraheme cytochrome *c*[24,25] or ion-gated transport in DNA.[26]

Conclusion

The approach reported herein 1) offers rather vast opportunities for the construction of novel phases upon variation of the nature of the amino acid (eventually a chiral residue attached to the redox core), 2) illustrates the benefit of engaging a templating base to control the chemical activity of ionizable residues during crystal growth, and 3) draws attention to the possibility that the overlap achieved between the HOMOs of a zwitterion and a neutral molecule is large enough to provide for significant delocalization despites their difference in energy.

We believe that the present report has significance that goes beyond the results obtained for **2** because it also illustrates issues such as relating the protonation state of ionizable residues[9,15] to their chemical activity, qualified herein by a proton-shared hydrogen bond, which is shown to be coupled to the electronic structure[27] and hole migration in the solid state,[28] and draws attention to electrostatic interactions that are of paramount importance in biology,[24–26,29–32] materials chemistry, and physics.[33,28]

Experimental Section

Synthesis of ethylenedithiotetrathiafulvaleneamidoethylglycinate (EDT-TTF-CO-NH-CH_2-CO_2Et): Triethylamine (1 mL) was added to ethylglycinate hydrochloride (0.500 g, 1.43 mmol) suspended in freshly distilled THF (20 mL) in a three-necked flask under nitrogen. A solution of ethylenedithiotetrathiafulvalene acid chloride[34] (0.500 g, 1.40 mmol) in THF (30 mL) was added dropwise. The reaction mixture was stirred overnight and THF was distilled under vacuum. The resulting mixture was extracted from water with dichloromethane (3×75 mL). The organic phases were collected, dried over sodium sulfate, and evaporated under vacuum to afford an orange–red solid. Crystallization from hot acetonitrile yielded orange–red single crystals that were suitable for X-ray diffraction studies.

Synthesis of 1: A solution of lithium hydroxide (0.02 g, 0.48 mmol) in water (3 mL) was added to a solution of EDT-TTF-CO-NH-CH_2-CO_2Et (0.17 g, 0.40 mmol) in 1,4-dioxane (20 mL). After stirring for 15 h at room temperature, hydrochloric acid (5 M, 5 mL) was added to the reaction mixture, which was stirred for a further 5 min. The crude product was extracted with ethyl acetate (3×50 mL). The organic layers were collected, dried over sodium sulfate, and evaporated to remove the solvent, but before the apparition of any solid. The concentrated mixture was allowed to evaporate slowly to yield tiny orange single crystals that were suitable for X-ray diffraction studies.

Synthesis of 2: Electrocrystallization[35] was carried out on EDT-TTF-CO-NH-CH_2-CO_2Et (5 mg) in a mixture of CH_2Cl_2/MeOH (11:1, v/v) containing tetrabutylammonium fumarate (45 mg) at a Pt-wire electrode in a two-compartment cell at a constant current and temperature of 0.2 μA and 303 K. Shiny black crystals, the formulation of which was obtained by determination of their crystal structure, were yielded after four weeks.

X-ray structure analysis of 1 and 2: Single-crystal data were collected at room temperature by using a Bruker Nonius KappaCCD diffractometer with monochromatized $Mo_{K\alpha}$ radiation ($\lambda = 0.71073$ Å; graphite monochromator, combined ϕ/ω scans). Empirical absorption correction of the experimental intensities was applied for all the data with the SADABS program.[36] The structures were solved by a direct method followed by Fourier syntheses and refined by a full-matrix least-squares method with the SHELX-97 programs.[37] All non-hydrogen atoms (except for methanol molecules in **2**) were refined in an anisotropic approximation. The positions of the hydrogen atoms were calculated with isotropic displacement parameters fixed at 120% (or 150% for $-CH_3$ and $-OH$ groups) of the corresponding parameters of the attached C, O, and N atoms. The coordinates of the H atoms were refined for all the non-disordered atoms. The crystallographic and refinement data are given in Table 1. CCDC-753662 and CCDC-753663 contain the supplementary crystallographic data for this paper. These data can be obtained free of charge from The Cambridge Crystallographic Data Centre via www.ccdc.cam.ac.uk/data_request/cif

Electronic structure calculations: The DFT band-structure calculations were carried out within the GGA[38] to the exchange-correlation energy. We used the Vienna ab initio simulation package (VASP)[39] and employed the projector-augmented wave (PAW)[40] methodology as implemented in the VASP code.[41] VASP uses a plane-wave basis set to represent the Kohn–Sham eigenstates and the electron density of the valence electrons. Herein, we have included in the basis set all the plane waves with kinetic energies up to 500 eV. The sampling of the Brillouin zone has been performed with a grid of 3×3×3 reciprocal space points generated according to the prescription of Monkhorst and Pack.[42] The tight-binding band-structure calculations were of the extended Hückel-type[43] with a modified Wolfsberg–Helmholtz formula to calculate the nondiagonal H_{mn} values.[44] The basis set consisted of double ζ Slater-type orbitals for C, N, O, and S atoms and single ζ Slater-type orbitals for the H atoms. The exponents, contraction coefficients, and ionization potentials were taken from previous reports.[8c, 45] All the calculations were carried out on a room-temperature crystal structure of **2**. The molecular electrostatic potentials were evaluated by means of B3LYP-DFT//6–31G* calculations with Gaussian 03, Revision D.02.[46]

Transport measurements: Resistivity was measured by a standard four-point method. The contacts were glued with silver epoxy adhesive on a single-crystal sample with dimensions of 0.2×0.2×0.01 mm. The measuring current was controlled during the measurements to keep the signal-to-noise ratio on acceptable level without heating up the sample.

ESR spectroscopic measurements: These were carried out on single crystals. For the low-frequency ESR measurements at 9.4 GHz, we used a commercially available Bruker ELEXSYS E500 spectrometer. The temperature was controlled by an Oxford ESR900 cryostat in the temperature range 4–300 K. Measurements in the millimeter wave frequency range were carried out on a home made quasioptical continuous-wave ESR spectrometer. The available microwave frequencies were 210, 315, and 420 GHz. The magnetic field (up to 16 T) was produced with an Oxford Instruments superconducting solenoid. We controlled the sample at the temperature range 2–300 K in a continuous-flow cryostat. More details about the spectrometer can be found elsewhere.[47]

Acknowledgements

L.Z. and S.S. gratefully acknowledge support from the CNRS and the Région Pays de la Loire for an associated researcher and postdoctoral position, respectively. Financial support from the ANR PNANO Project TTF-Based Nanomat ANR-07-NANO-030-01 is gratefully acknowledged. Work at Bellaterra was supported by the DGES-Spain (Project FIS2009-12721-C04-03 and CSD2007-00041). Some of the computational experiments were carried out by using the facilities of CESCA and CESGA. Work at Barcelona was supported by the DGES-Spain (FIS2008-03845) and Generalitat de Catalunya (2009SGR-1309). Work at Lausanne was supported by the NCCR Manep of the Swiss National Science Foundation.

[1] S. Booth, E. N. K. Wallace, K. Singhak, P. N. Barlett, J. D. Kilburn, *J. Chem. Soc. Perkin Trans. 1* **1998**, 1467–1474.
[2] A. S. Batsanov, S. L. Viles, A. J. Moore, *Acta Crystallogr. Sect. E* **2005**, *61*, 648–650.
[3] a) M. Giffard, A. Riou, G. Mabon, N. Mercier, P. Molinie, T. Phap Nguyen, *J. Mater. Chem.* **1999**, *9*, 851–853; b) N. Mercier, M. Giffard, G. Pilet, M. Allain, P. Hudhomme, G. Mabon, E. Levillain, A. Gorgues, A. Riou, *J. Chem. Soc. Chem. Commun.* **2001**, 2722; c) Y. Lakhdar, A. El-Ghayoury, L. Zorina, N. Mercier, M. Allain, C. Mézière, P. Auban-Senzier, P. Batail, M. Giffard, *Eur. J. Inorg. Chem.* **2010**, 3338—3342.
[4] P. Gilli, L. Pretto, V. Bertolasi, G. Gilli, *Acc. Chem. Res.* **2009**, *42*, 33–44.
[5] G. D. Cymes, Y. Li, C. Grosman, *Nature* **2005**, *438*, 975–980.
[6] M. Fourmigué, P. Batail, *Chem. Rev.* **2004**, *104*, 5379–5418.
[7] P. García, S. Dahaoui, C. Katan, M. Souhassou, C. Lecomte, *Faraday Discuss.* **2007**, *135*, 217–235.
[8] a) S. A. Baudron, P. Batail, C. Rovira, E. Canadell, R. Clérac, *Chem. Commun.* **2003**, 1820–1821; b) S. A. Baudron, N. Avarvari, P. Batail, C. Coulon, R. Clérac, E. Canadell, P. Auban-Senzier, *J. Am. Chem. Soc.* **2003**, *125*, 11583–11590; c) S. A. Baudron, N. Avarvari, E. Canadell, P. Auban-Senzier, P. Batail, *Chem. Eur. J.* **2004**, *10*, 4498–4511.
[9] J. Yuasa, S. Yamada, S. Fukuzumi, *J. Am. Chem. Soc.* **2008**, *130*, 5808–5820.
[10] O. F. Mohammed, O.-H. Kwon, C. M. Othon, A. H. Zewail, *Angew. Chem.* **2009**, *121*, 6369–6374; *Angew. Chem. Int. Ed.* **2009**, *48*, 6251–6256.
[11] Y. Li, G. Li, X. Wang, W. Li, Z. Su, Y. Zhang, Y. Ju, *Chem. Eur. J.* **2009**, *15*, 6399–6407.
[12] X. Zhao, S. Zhang, *Chem. Soc. Rev.* **2006**, *35*, 1105–1110.
[13] J. S. Nowick, *Acc. Chem. Res.* **2008**, *41*, 1319–1330.
[14] G. Angelici, G. Falini, H.-J. Hofmann, D. Huster, M. Monari, C. A. Tomasini, *Angew. Chem.* **2008**, *120*, 8195–8198; *Angew. Chem. Int. Ed.* **2008**, *47*, 8075–8078.
[15] A. Adhikary, A. Kumar, D. Khanduri, M. D. Sevilla, *J. Am. Chem. Soc.* **2008**, *130*, 10282–10292.
[16] A. Dolbecq, M. Fourmigué, F. Krebs, P. Batail, E. Canadell, R. Clérac, C. Coulon, *Chem. Eur. J.* **1996**, *2*, 1275–1282.
[17] T. Murata, Y. Morita, Y. Yakiyama, Y. Nishimura, T. Ise, D. Shiomi, K. Sato, T. Takui, K. Nakasuji, *Chem. Commun.* **2007**, 4009–4011.
[18] Y. Morita, Y. Yamamoto, Y. Yakiyama, T. Murata, K. Nakasuji, *Chem. Lett.* **2008**, *37*, 24–25.
[19] E.-K. Schillinger, E. Mena-Osteritz, J. Hentschel, H. G. Börner, P. Baüerle, *Adv. Mater.* **2009**, *21*, 1562–1567.
[20] J.-I. Yamada, H. Akutsu, H. Nishikawa, K. Kikuchi, *Chem. Rev.* **2004**, *104*, 5057–5083.
[21] A. D. Buckingham, J. E. Del Bene, S. A. C. McDowell, *Chem. Phys. Lett.* **2008**, *463*, 1–10.
[22] G. Gilli, P. Gilli in *The Nature of the Hydrogen Bond: Outline of a Comprehensive Hydrogen Bond Theory*, Oxford University Press, New York, **2009**, p. 318.
[23] M.-H. Whangbo, J. M. Williams, P. C. W. Leung, M. A. Beno, T. J. Emge, H. H. Wang, *Inorg. Chem.* **1985**, *24*, 3500–3502.
[24] H. Akutsu, Y. Takayama, *Acc. Chem. Res.* **2007**, *40*, 171–177.
[25] G. Brändén, M. Brändén, B. Schmidt, D. A. Mills, S. Ferguson-Miller, P. Brzezinski, *Biochemistry* **2005**, *44*, 10466–10474.
[26] R. N. Barnett, C. L. Cleveland, A. Joy, U. Landman, G. B. Schuster, *Science* **2001**, *294*, 567–571.
[27] R. Rousseau, M. Gener, E. Canadell, *Adv. Funct. Mater.* **2004**, *14*, 201–214.
[28] T. Giamarchi, *Chem. Rev.* **2004**, *104*, 5037–5055.
[29] M. E. Davis, J. A. McCammon, *Chem. Rev.* **1990**, *90*, 509–521.
[30] K. Harada, M. Makino, H. Sugimoto, S. Hirota, T. Matsuo, Y. Shiro, Y. Hisaeda, T. Hayashi, *Biochemistry* **2007**, *46*, 9406–9416.
[31] F. C. Grozema, S. Tonzani, Y. A. Berlin, G. C. Schatz, L. D. A. Siebbeles, M. A. Ratner, *J. Am. Chem. Soc.* **2008**, *130*, 5157–5166.
[32] I. Levental, A. Cebers, P. A. Janmey, *J. Am. Chem. Soc.* **2008**, *130*, 9025–9030.
[33] L. Zorina, S. Simonov, C. Mézière, E. Canadell, S. Suh, S. E. Brown, P. Foury-Leylekian, P. Fertey, J.-P. Pouget, P. Batail, *J. Mater. Chem.* **2009**, *19*, 6980–6994.
[34] K. Heuzé, M. Fourmigué, P. Batail, *J. Mater. Chem.* **1999**, *9*, 2373–2379.
[35] P. Batail, K. Boubekeur, M. Fourmigué, J.-C. P. Gabriel, *Chem. Mater.* **1998**, *10*, 3005–3015.
[36] SADABS, G. M. Sheldrick, University of Göttingen (Germany), **1996**.
[37] G. M. Sheldrick, *Acta Crystallogr. Sect. A* **2008**, *64*, 112–122.
[38] J. P. Perdew, K. Burke, M. Ernzerhof, *Phys. Rev. Lett.* **1996**, *77*, 3865–3868.
[39] G. Kresse, J. Furthmüller, *Phys. Rev. B* **1996**, *54*, 11169–11185.
[40] P. E. Blöchl, *Phys. Rev. B* **1994**, *50*, 17953–17979.
[41] G. Kresse, D. Joubert, *Phys. Rev. B* **1999**, *59*, 1758–1775.
[42] H. J. Monkhorst, J. D. Pack, *Phys. Rev. B* **1976**, *13*, 5188–5192.
[43] M.-H. Whangbo, R. Hoffmann, *J. Am. Chem. Soc.* **1978**, *100*, 6093–6098.
[44] J. H. Ammeter, H.-B. Bürgi, J. Thibeault, R. Hoffmann, *J. Am. Chem. Soc.* **1978**, *100*, 3686–3692.
[45] A. Pénicaud, K. Boubekeur, P. Batail, E. Canadell, P. Auban-Senzier, D. Jérome, *J. Am. Chem. Soc.* **1993**, *115*, 4101–4112.
[46] Gaussian 03, Revision C.02, M. J. Frisch, G. W. Trucks, H. B. Schlegel, G. E. Scuseria, M. A. Robb, J. R. Cheeseman, J. A. Montgomery, Jr., T. Vreven, K. N. Kudin, J. C. Burant, J. M. Millam, S. S. Iyengar, J. Tomasi, V. Barone, B. Mennucci, M. Cossi, G. Scalmani, N. Rega, G. A. Petersson, H. Nakatsuji, M. Hada, M. Ehara, K. Toyota, R. Fukuda, J. Hasegawa, M. Ishida, T. Nakajima, Y. Honda, O. Kitao, H. Nakai, M. Klene, X. Li, J. E. Knox, H. P. Hratchian, J. B. Cross, V. Bakken, C. Adamo, J. Jaramillo, R. Gomperts, R. E. Stratmann, O. Yazyev, A. J. Austin, R. Cammi, C. Pomelli, J. W. Ochterski, P. Y. Ayala, K. Morokuma, G. A. Voth, P. Salvador, J. J. Dannenberg, V. G. Zakrzewski, S. Dapprich, A. D. Daniels, M. C. Strain, O. Farkas, D. K. Malick, A. D. Rabuck, K. Raghavachari, J. B. Foresman, J. V. Ortiz, Q. Cui, A. G. Baboul, S. Clifford, J. Cioslowski, B. B. Stefanov, G. Liu, A. Liashenko, P. Piskorz, I. Komaromi, R. L. Martin, D. J. Fox, T. Keith, M. A. Al-Laham, C. Y. Peng, A. Nanayakkara, M. Challacombe, P. M. W. Gill, B. Johnson, W. Chen, M. W. Wong, C. Gonzalez, and J. A. Pople, Gaussian, Inc., Wallingford CT, **2004**.
[47] B. Náfrádi, R. Gaál, T. Fehér, L. Forró, *J. Magn. Reson.* **2008**, *192*, 265–268.

Received: July 2, 2010
Published online: October 28, 2010

